

Instability and evolution of the magnetic ground state in metallic perovskites $\text{GdRh}_3\text{C}_{1-x}\text{B}_x$

Abhishek Pandey,^{1,*} A. K. Singh,² Shovan Dan,³ K. Ghosh,⁴ I. Das,⁵ S. Tripathi,²
U. Kumar,⁶ R. Ranganathan,⁵ D. C. Johnston,⁷ and Chandan Mazumdar⁵

¹*School of Physics, University of the Witwatersrand, Johannesburg, Gauteng 2000, South Africa*

²*Department of Physics, Indian Institute of Technology, Varanasi, Uttar Pradesh 221005, India*

³*Department of Physics, University of Burdwan, Burdwan, Bengal 713104, India*

⁴*Department of Physics, P. C. Vigyan College, Chapra, Bihar 841301, India*

⁵*Condensed Matter Physics Division, Saha Institute of Nuclear Physics, Kolkata, Bengal 700064, India*

⁶*Department of Physics, National Institute of Technology, Jamshedpur, Jharkhand 831014, India*

⁷*Ames Laboratory-USDOE and Department of Physics and Astronomy, Iowa State University, Ames, Iowa 50011, USA*

(Dated: March 3, 2020)

We report investigations of the structural, magnetic, electrical transport and thermal properties of five compositions of the metallic perovskite $\text{GdRh}_3\text{C}_{1-x}\text{B}_x$ ($0.00 \leq x \leq 1.00$). Our results show that all the five compositions undergo magnetic ordering at low temperatures, but the nature of the ordered state is significantly different in the carbon- and the boron-rich compositions, where the former shows signatures of an amplitude-modulated magnetic structure and the latter exhibits evidences of an equal-moment incommensurate antiferromagnetic ordering. We also observe a remarkable field-dependent evolution of conduction carrier polarization in the compositionally disordered compounds. The outcomes indicate that this system is energetically situated in proximity to a magnetic instability where small variations in the control parameter(s), such as lattice constant and/or electron density, lead to considerably different ground states.

PACS numbers: 75.30.-m, 75.25.-j, 72.15.Eb

INTRODUCTION

Perovskite is one of the most well-studied crystal structure classes [1, 2]. Materials crystallizing in this relatively simple structure exhibit many intriguing physical phenomena as well as application-oriented properties. Usually, while referring to a perovskite compound one means ABO_3 -type oxygen-containing material. However, there are several non-oxide perovskite materials that host a transition metal ion in the place of oxygen at the face-center lattice sites of the cubic unit cell, and those are usually referred to as “*metallic perovskites*”. MgCNi_3 [3], RhFe_3N [4, 5], Sc_3MC ($M = \text{Al, Ga, In, Tl}$) [6], Mn_3GaC [7–9] and RT_3X ($R = \text{rare earth ion; } T = \text{Pd, Rh; } X = \text{B, C}$) [10–18] are some of the noted metallic perovskites that have been thoroughly investigated and several exciting properties such as superconductivity, giant magnetoresistance (MR), anomalous thermal expansion, magnetocaloric effect, tunable valence behavior and temperature-independent electrical resistivity have been observed. Interestingly, several binary RT_3 compounds related to the RT_3X perovskites also crystallize in the structurally related cubic AuCu_3 phase, where the body-center site remains vacant [19–23]. One such compound GdPd_3 has recently been reported for its exciting oscillating MR behavior that arises because of the extremely fragile magnetic structure of the material [24]. Binary GdRh_3 , however, does not form in a melt-separable equilibrium phase [25], but the related GdRh_3B and GdRh_3C phases are reported to crystallize in an undistorted per-

ovskite structure [16, 18]. Preliminary results reported on GdRh_3X suggest considerably difference properties of the boron- and the carbon-containing compounds [16].

We present in this paper an investigation of five compositions of $\text{GdRh}_3\text{C}_{1-x}\text{B}_x$ ($x = 0, 0.25, 0.50, 0.75, 1.00$) and find a systematic evolution of the properties that is apparently linked to the changes in the lattice parameter as well as in the electron count of the system, both of which are altered when C is substituted by B. Our results indicate an evolution of the magnetic structure from amplitude modulated (AM) one in GdRh_3C to an equal-moment (EM) structure in GdRh_3B . This outcome, which is triggered by tweaking the relative compositions of small nonmagnetic metalloids B and C in a compound that hosts heavy rare-earth and transition metal elements, hints that the ground states of these phases are formed near a magnetic tipping point where a small perturbation to the parameter(s) can destabilize the energy balance and lead to a considerably different new ground state.

EXPERIMENTAL DETAILS

Samples were synthesized by arc-melting the stoichiometric amounts of highly pure (purity $\geq 99.9\%$) constituent elements from Alfa-Aesar in an inert atmosphere of argon. Post melting, the samples were wrapped in Ta foils and annealed at 1000°C for 240 h under vacuum. Structural characterization of the samples was performed by refining temperature dependent x-ray diffrac-

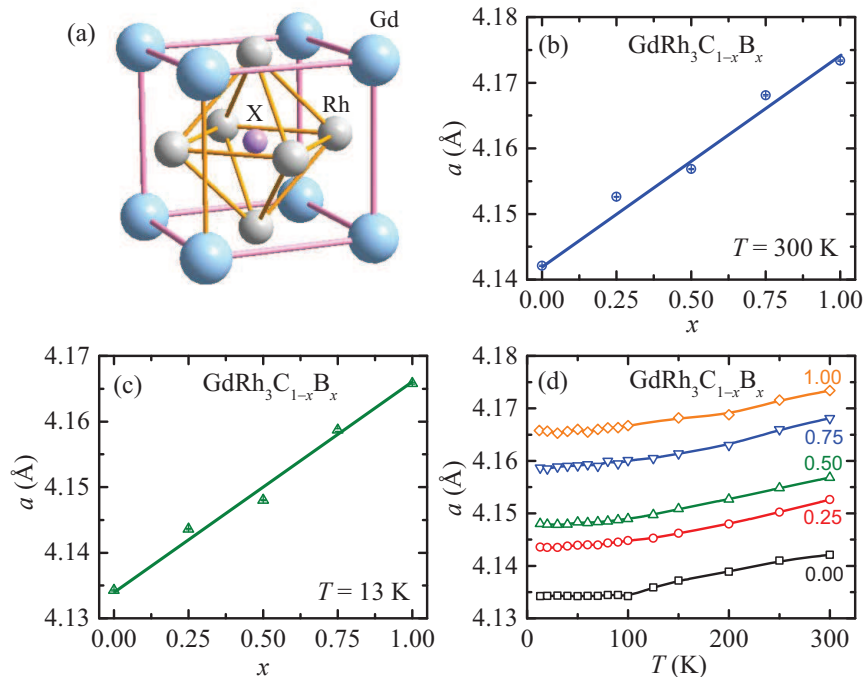


FIG. 1: (a) Arrangement of Gd, Rh and X atoms in the cubic unit cell of GdRh_3X ($X = \text{B}$ and C). Variation of the cubic unit cell parameter a with the boron concentration x at temperatures $T = 300$ and 13 K is shown in (b) and (c), respectively. Solid lines in (b) and (c) are guides to the eye. (d) The temperature dependence of a of the five $\text{GdRh}_3\text{C}_{1-x}\text{B}_x$ compositions, where the x is indicated next the respective plots. Sizes of the error bars in (b), (c) and (d) are smaller than the size of the symbols.

tion (XRD) data collected between 13 and 300 K using a TTRAX-III high-resolution powder diffractometer of Rigaku Inc., Japan, which is equipped with a rotating-anode Cu x-ray source. The FullProf package [26] was used for Rietveld refinements of the powder XRD data collected at fifteen different temperatures on the five investigated compositions. Temperature- and magnetic field-dependent magnetization M measurements under zero field-cooled conditions were carried out utilizing a Magnetic Properties Measurement System of Quantum Design, Inc., USA. Heat capacity C_p data were collected using a Physical Properties Measurement System of Quantum Design, Inc., USA. Electrical transport measurements were performed between the temperatures 2 and 300 K using a home-built multisample probe installed in a cryostat supplied by Oxford Inc., UK.

RESULTS

Crystal structure and lattice parameter

The room temperature powder XRD data of $\text{GdRh}_3\text{C}_{1-x}\text{B}_x$ ($x = 0, 0.25, 0.50, 0.75$ and 1) show that all five investigated compositions crystallize in the cubic perovskite structure (space group: $Pm\bar{3}m$, No.: 221) shown in Fig. 1(a). Additionally, the XRD data taken at fifteen different temperatures between 13 and 300 K show

that the materials remain in a single phase at all temperatures within the aforementioned temperature range (Fig. S1). The results show that the cubic lattice parameter a deduced from Rietveld analysis of the XRD data nicely follows Vegard's law [27], both at 13 K as well as at 300 K, where a increases linearly with boron content x [Figs. 1(b) and (c)]. This observation is a confirmation of full solubility of the carbon and the boron compounds and also provides additional evidence for the single-phase nature of all the compositions. Figure 1(d) shows that while the lattice parameters of the four compositions $\text{GdRh}_3\text{C}_{1-x}\text{B}_x$ ($x = 0.25, 0.50, 0.75$ and 1) exhibit a positive thermal expansion between 13 and 300 K, that of GdRh_3C displays nearly zero thermal expansion up to ~ 100 K, and then shows a positive thermal expansion but with a pronounced negative curvature. As the anomaly observed in GdRh_3C occurs at quite high temperatures, we anticipate that it has a nonmagnetic origin and is most likely related to the energy balance between the bonding strengths and/or the elastic couplings and anharmonicity of the pair potential that leads to positive thermal expansion. A result suggesting a substantial dependence of the micro-Vickers hardness on the boron content in GdRh_3B_x compounds was reported earlier [28].

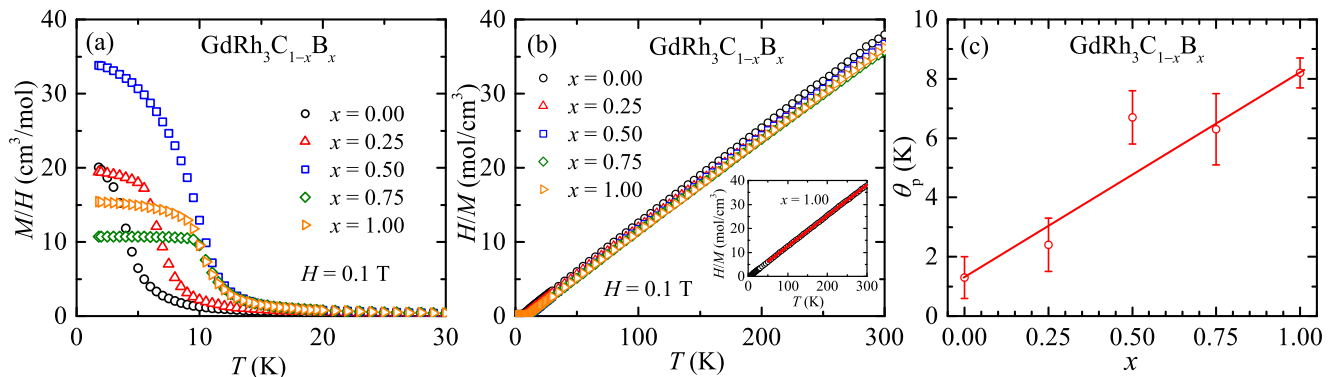


FIG. 2: (a) Magnetic susceptibility $\chi \equiv M/H$ versus temperature T of the five $\text{GdRh}_3\text{C}_{1-x}\text{B}_x$ compositions. (b) Inverse susceptibility χ^{-1} versus T plot for the same five compositions. Inset: the $\chi^{-1}(T)$ plot of GdRh_3C . Solid line is the Curie-Weiss fit using $\chi = C/(T - \theta_p)$, where C is the Curie constant and θ_p is the Weiss temperature. (c) Variation of θ_p with boron concentration x . The solid line is a guide to the eye.

TABLE I: Parameters obtained from the analysis of powder x-ray diffraction $I(2\theta)$, magnetic susceptibility $\chi(T)$, magnetization $M(H)$, heat capacity $C_p(T)$ and electrical resistivity $\rho(T)$ data of $\text{GdRh}_3\text{C}_{1-x}\text{B}_x$ ($x = 0.00, 0.25, 0.50, 0.75$ and 1.00) and the nonmagnetic analogue compound YRh_3B . The listed parameters are the lattice parameter a , paramagnetic Weiss temperature θ_p , effective paramagnetic moment μ_{eff} , magnetic moment $\mu_{5.5 \text{ T}}$ at $H = 5.5 \text{ T}$, highest measured value of magnetic moment μ_{max} for $H \leq 5.5 \text{ T}$, Debye temperature Θ_D and Einstein temperature Θ_E . The fractional contribution u of the Einstein term to the $C_p(T)$ is given in parenthesis below the respective values of the Θ_E . The magnetic ordering temperatures T_M , T_H and T_R obtained from the $\chi(T)$, $C_p(T)$ and $\rho(T)$ measurements, respectively, are listed under the column marked by T^* .

Compound	a (Å)	θ_p (K)	μ_{eff} (μ_B)	$\mu_{5.5 \text{ T}}$ ($\mu_B/\text{f.u.}$)	μ_{max} ($\mu_B/\text{f.u.}$)	Θ_D (K)	Θ_E (K)	T^* (K)	
GdRh_3C	13 K: 4.1343(1)	1.3(7)	7.95(5)	7.01	7.01	522(21)	158(3)	$T_M = 3.3(2)$	
	300 K: 4.1421(1)							$[u = 0.49(3)]$	$T_H = 3.3(1)$
									$T_R = 3.3(5)$
$\text{GdRh}_3\text{C}_{0.75}\text{B}_{0.25}$	13 K: 4.1436(1)	2.4(9)	8.08(3)	6.92	7.53	554(27)	158(3)	$T_M = 5.5(1)$	
	300 K: 4.1526(1)							$[u = 0.51(3)]$	$T_H = 5.4(1)$
									$T_R = 7.4(2)$
$\text{GdRh}_3\text{C}_{0.50}\text{B}_{0.50}$	13 K: 4.1480(7)	6.7(9)	8.00(6)	6.42	7.08	526(18)	154(3)	$T_M = 9.0(2)$	
	300 K: 4.1568(2)							$[u = 0.45(3)]$	$T_H = 9.7(1)$
									$T_R = 10.6(1)$
$\text{GdRh}_3\text{C}_{0.25}\text{B}_{0.75}$	13 K: 4.1587(2)	6.3(1)	8.11(6)	6.57	7.23	517(21)	158(3)	$T_M = 10.0(1)$	
	300 K: 4.1681(1)							$[u = 0.49(3)]$	$T_H = 9.9(1)$
									$T_H = 10.8(1)$
GdRh_3B	13 K: 4.1658(1)	8.2(5)	8.05(2)	6.92	6.92	516(21)	157(3)	$T_M = 9.5(1)$	
	300 K: 4.1734(1)							$[u = 0.48(3)]$	$T_H = 9.4(1)$
									$T_{R1} = 11.9(1)$
YRh_3B	300 K: 4.1647(2)	—	—	—	—	551(12)	171(2)	$T_{R2} = 10.0(1)$	
								$[u = 0.48(2)]$	

Magnetic properties

The magnetic susceptibilities $\chi \equiv M/H$ of the five $\text{GdRh}_3\text{C}_{1-x}\text{B}_x$ compounds at low temperatures ($T \leq 30 \text{ K}$) are shown in Fig. 2(a). The shapes and magnitudes of the $\chi(T)$ plots suggest ferromagnetic (FM) ordering in all five samples, but with considerably different

magnetic ordering temperatures T_M that range between ~ 3 and 10 K (Table I). The linear variation of the inverse susceptibility χ^{-1} with temperature for $T \gtrsim T_M$ indicates the presence of local magnetic moments in the materials that follow the Curie-Weiss law in the paramagnetic T -region [Fig. 2(b)]. The fitted values of the effective paramagnetic moment μ_{eff} and the Weiss tem-

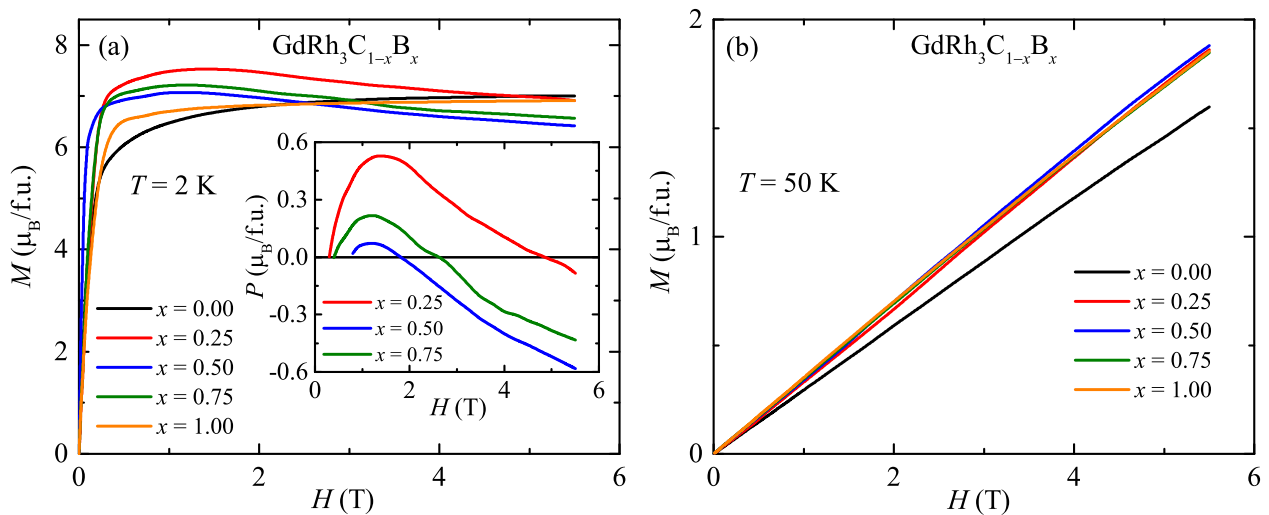


FIG. 3: Magnetization M versus applied magnetic field H plots of the five $\text{GdRh}_3\text{C}_{1-x}\text{B}_x$ compositions at $T = 2$ and 50 K are shown in (a) and (b), respectively. Inset in (a) shows the evolution of conduction electron polarization P for $x = 0.25, 0.50$ and 0.75 compositions, which has been extracted by subtracting $7 \mu_B$ from the measured M , with H .

perature θ_p in the Curie-Weiss law are listed in Table I. The estimated value of μ_{eff} of GdRh_3C agrees with the expectation ($7.94 \mu_B$) for the spin $S = 7/2$ Gd^{+3} ion with g -factor $g = 2$. However, the values of μ_{eff} in the remaining four compositions are slightly larger than expected, which apparently is due to partial polarization of the conduction carriers [29–35]. The θ_p varies almost linearly with the boron content [Fig. 2(c)]; a fact which shows that boron incorporation and the resultant lattice expansion manifests into a significant alteration of the strength of the resultant magnetic interaction in the compound. It also suggests that likely there are competing magnetic interactions present in these materials, and a minute tweaking of the parameters, such as, the distance between the magnetic Gd^{+3} ions and/or the change in conduction carrier density induced by doping holes by replacing C with B can alter their energy balance and could possibly lead to different magnetic ground states.

Figure 3(a) shows isothermal magnetization M versus magnetic field H data of the five $\text{GdRh}_3\text{C}_{1-x}\text{B}_x$ compositions measured at $T = 2$ K below their respective magnetic ordering temperatures (Table I). The M of the two end compositions, GdRh_3C and GdRh_3B , monotonically increases with increasing H and then saturates at high fields, exhibiting a behavior which is often observed in Gd^{+3} ferromagnets. While $M(H)$ data of the two compounds are qualitatively similar, they are significantly different at the low fields where the former shows a slow saturation to $\mu = 7 \mu_B$ but the latter attains this value, which is expected from the $S = 7/2$ Gd^{+3} ions, at relatively lower field of ≈ 0.5 T [Fig. 3(a)]. The $M(H)$ data of the other three compositions $x = 0.25, 0.50$ and 0.75 are substantially different. The M in these three compositions first increases sharply with increasing H ,

then shows a broad peak, and then starts decreasing with the further increase of H . The maximum moment values μ_{max} that these three compositions attain are significantly larger than possible solely from the Gd^{+3} ions (Table I), indicating that a sizable field-dependent contribution to the measured moment is coming from polarization P of the conduction carriers [29–35]. The μ_{max} is largest in $\text{GdRh}_3\text{C}_{0.75}\text{B}_{0.25}$, where it attains a value of $7.53 \mu_{\text{eff}}$ (Table I), suggesting that the P contributes up to $0.53 \mu_{\text{eff}}$ to the observed moment in this composition in the explored applied field range [Inset, Fig. 3]. This value is in good agreement with the polarization $0.6 \pm 0.1 \mu_{\text{eff}}$ reported in literature for Gd metal [29–34]. The nonmonotonic behavior of the $M(H)$ data suggests that the P is strongly field dependent in these three compounds. Furthermore, $P(H)$ plot shows a crossover from positive to negative values at the sample-dependent H s [Inset, Fig. 3], suggesting that along with the magnitude its orientation relative to the localized moments also evolves with H , which is a remarkable result. Additionally, the fact that the field-dependence of P occurs only in the compositions where either boron or carbon is partially substituted hints that this phenomenon is apparently linked with the lattice disorder introduced by the substitution and the resultant modification of the local interactions. As expected in the paramagnetic state of localized moments, the $M(H)$ plots are linear at $T = 50$ K [Fig. 3(b)]. The $M(H)$ of the $\text{GdRh}_3\text{C}_{1-x}\text{B}_x$ compounds at three different temperatures are shown in the Figure S2 of Supplementary Materials.

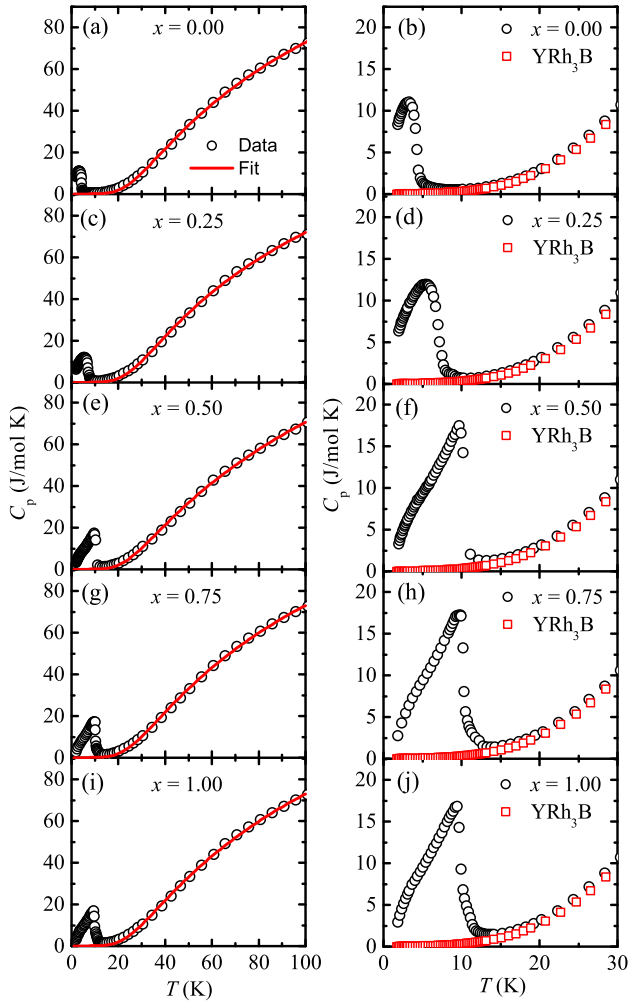


FIG. 4: Left panel: Heat capacity C_p versus temperature T data of the five $\text{GdRh}_3\text{C}_{1-x}\text{B}_x$ compositions. Solid red curves in the left panel figures are the fits of the $C_p(T)$ data using the Debye-Einstein model as discussed in the text. Right panel: Low-temperature ($T \leq 30$ K) $C_p(T)$ data of the $\text{GdRh}_3\text{C}_{1-x}\text{B}_x$ compositions are shown along with the $C_p(T)$ data of the nonmagnetic analogue compound YRh_3B . The temperature axis of the $C_p(T)$ data of YRh_3B was scaled to incorporate the difference in its molar mass compared to the $\text{GdRh}_3\text{C}_{1-x}\text{B}_x$ compounds [24].

Heat capacity and magnetic entropy

The heat capacity $C_p(T)$ data of the five $\text{GdRh}_3\text{C}_{1-x}\text{B}_x$ compositions shown in the left panel of Fig. 4 demonstrate the occurrence of magnetic transitions at their respective ordering temperatures T_H . The high-temperature ($T > T_H$) $C_p(T)$ data could not be fitted satisfactorily using solely the Debye model of acoustic phonons (Fig. S3, Supplementary Material), but the fit improved significantly by employing the single-frequency Einstein term along with the Debye model [36] (left panels, Fig. 4). The estimated Debye

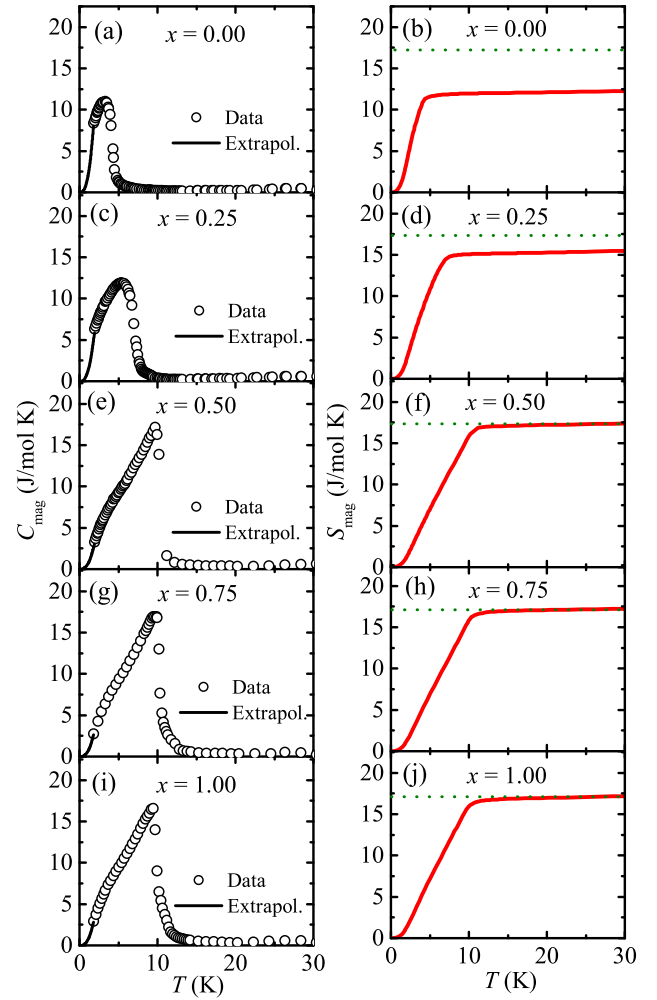


FIG. 5: Left panel: Magnetic contribution $C_{\text{mag}} = C_p - C_{\text{YRh}_3\text{B}}$ to the capacity of the five $\text{GdRh}_3\text{C}_{1-x}\text{B}_x$ compositions, where $C_{\text{YRh}_3\text{B}}$ is the heat capacity of the non-magnetic analogue YRh_3C . Solid curves are the extrapolation of the experimental data down to $T = 0$ K using the expression $C_{\text{mag}} = BT^3$. Right panel: Magnetic entropy $S_{\text{mag}} = \int_0^T \frac{C_{\text{mag}}}{T} dT$ of the respective compositions. Dashed green horizontal lines in the figures represent the entropy $R \ln(2S + 1) = 17.3$ J/mol K associated with the Gd^{+3} spins $S = 7/2$.

temperature Θ_D , the Einstein temperature Θ_E and the fractional contribution of the Einstein term are all listed in Table I. The low-temperature ($T \leq 30$ K) $C_p(T)$ data of the $\text{GdRh}_3\text{C}_{1-x}\text{B}_x$ compositions are shown along with the $C_p(T)$ data of the nonmagnetic reference compound YRh_3B in the respective right panels of Fig. 4. The data for the boron-rich compositions ($x = 0.50, 0.75$ and 1.00) show a narrow peak centered at T_H and a shoulder at lower temperature. This behavior is expected from an equal moment (EM) local moment system under the mean-field model [38–41]. However, the $C_p(T)$ data of the carbon-rich compositions ($x = 0.00$ and 0.25) exhibit a significantly different behavior in that they show a

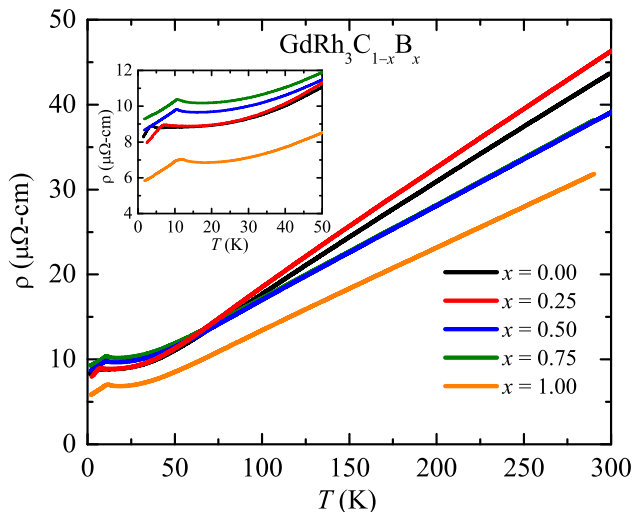


FIG. 6: Electrical resistivity ρ versus temperature T of the five $\text{GdRh}_3\text{C}_{1-x}\text{B}_x$ compositions. Inset: The $\rho(T)$ data at low temperatures $T \leq 50$ K.

broad peak centered at their T_{H} , which is qualitatively different from the λ -shaped peaks observed in the three boron-rich compositions. Such broad transitions have been reported in several Gd-based materials and are a characteristic signature of amplitude modulated (AM) magnetic structures [40–43]. Molecular field theory predicts that the discontinuity in C_{mag} for equal moment systems with a spin $S = 7/2$ at the magnetic ordering temperature is $\Delta C_{\text{mag}} = 21.14$ J/mol K [37, 41]. The observed ΔC_{mag} is 16.6(3) and 11.5(5) J/mol K in the boron- and the carbon-rich compositions, respectively. The smaller than expected ΔC_{mag} observed in the boron-rich compositions is likely due to the presence of substantial short-ranged correlations that start building up above the respective T_{HS} [Fig. 4].

The magnetic contributions to the heat capacities estimated using $C_{\text{mag}}(T) = C_{\text{p}}(T) - C_{\text{YRh}_3\text{B}}(T)$ are shown in the left panels of Fig. 5. The C_{mag} below 1.8 K was extrapolated using $C_{\text{mag}} = BT^3$, applicable for antiferromagnetic (AFM) spin waves [44], where B is a constant. The magnetic entropy S_{mag} of the boron rich compositions ($x = 0.50, 0.75$ and 1.00) saturates to $R \ln(2S + 1) = R \ln 8 = 17.3$ J/mol K at around 10 K as expected for a $S = 7/2$ system (Fig. 5), where R is the molar gas constant. However, the S_{mag} of the carbon rich compositions ($x = 0.00$ and 0.25) appear to saturate at values which are significantly smaller than $R \ln 8$. This observation indicates that not all the Gd spins are ordering at the respective T_{HS} of these compositions, and there is likely a residual entropy confined at the lower temperatures. Thus, our $C_{\text{mag}}(T)$ and $S_{\text{mag}}(T)$ data collectively indicate that underlying magnetic ground state in $\text{GdRh}_3\text{C}_{1-x}\text{B}_x$ compounds undergoes a notable transformation between $x = 0.25$ and 0.50 .

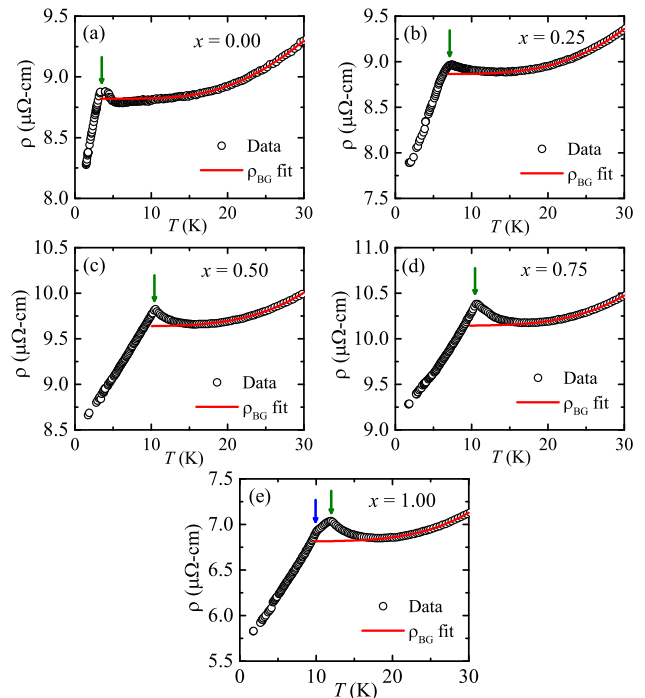


FIG. 7: Electrical resistivity ρ versus temperature T of the $\text{GdRh}_3\text{C}_{1-x}\text{B}_x$ compositions with $x = 0.00, 0.25, 0.50, 0.75$ and 1.00 at low temperatures $T \leq 30$ K are plotted in (a), (b), (c), (d) and (e), respectively. The magnetic ordering temperature T_{R} is indicated by the vertical green arrows in (a), (b), (c) and (d). While in (e), the green and blue arrows represent T_{R1} and T_{R2} , respectively. Red curves are the Bloch-Grüneisen fits of the $\rho(T)$ data performed for $T \geq 15$ K, and then extrapolated down to low temperatures.

Electrical resistivity

The electrical resistivities ρ of all five $\text{GdRh}_3\text{C}_{1-x}\text{B}_x$ compositions show metallic T -dependences at temperatures $T \gtrsim T_{\text{R}}$ (Fig. 6), where T_{R} is the magnetic ordering temperature deduced from the $\rho(T)$ data. The high-temperature $\rho(T)$ data were fitted satisfactorily using the Bloch-Grüneisen model of electrical transport in metals (Fig. S5). At low temperatures, the $\rho(T)$ data of the $x = 0.25, 0.50$ and 0.75 compositions exhibit well-defined peaks at their respective T_{RS} (Table I), below which the $\rho(T)$ decreases sharply with the decrease of T [Fig. 7 (b)–(d)]. The $\rho(T)$ of GdRh_3C shows a kink at T_{R1} and then an additional peak at T_{R2} [Fig. 7 (e)]. However, the low- T $\rho(T)$ behaviors of GdRh_3C is different; it exhibits a small and broad hump at its T_{R} [Fig. 7 (a)], and then decreases sharply with the decrease of T . The sharp decrease in the $\rho(T)$ data observed in all five compositions below their respective T_{RS} is due to the reduction in the spin disorder scattering in the magnetically ordered states.

To extract the magnetic contribution ρ_{mag} contained in the observed $\rho(T)$ peaks of the $\text{GdRh}_3\text{C}_{1-x}\text{B}_x$ compositions, we subtracted the fitted Bloch-Grüneisen re-

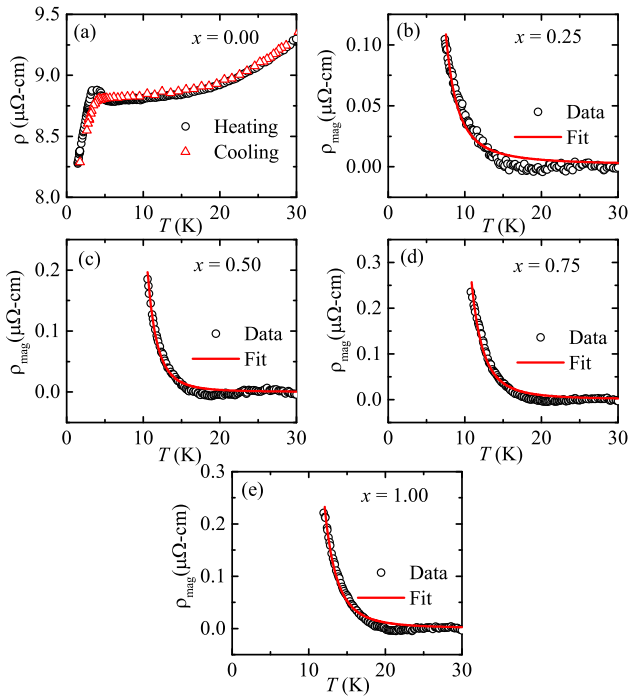


FIG. 8: (a) Electrical resistivity ρ versus temperature T of GdRh_3C for $T \leq 30$ K for both heating and cooling cycles. The magnetic contributions to the resistivities $\rho_{\text{mag}} = \rho - \rho_{\text{BG}}$ versus T of $\text{GdRh}_3\text{C}_{1-x}\text{B}_x$ compositions with $x = 0.25, 0.50, 0.75$ and 1.00 for $T_{\text{R}} \leq T \leq 30$ K are plotted in (b), (c), (d) and (e), respectively, where ρ_{BG} is the non-magnetic Bloch-Grüneisen contribution to the resistivity as discussed in the text and T_{R} is the magnetic ordering temperature obtained from the resistivity measurement as indicated in by the vertical arrows in Fig. 7. The red curves are fits using the expression discussed in the text.

sistivity ρ_{BG} from the experimental data (Fig. 7). The temperature variation of $\rho_{\text{mag}} = \rho - \rho_{\text{BG}}$ is shown in the Figs. 8 (b)–(e) for $x = 0.25, 0.50, 0.75$ and 1.00 , respectively. Because of the shallow hump observed in the $\rho(T)$ of GdRh_3C , it was not meaningful to do this analysis on this compound. Instead, we have plotted the thermal hysteresis data on GdRh_3C [Fig. 8(a)], which shows that the shallow peak disappears when the $\rho(T)$ data are taken while cooling the sample from above its magnetic ordering temperature. This suggests the presence of some kind of spin or domain blocking accompanied with the magnetic order in this compound. A similar observation was reported earlier in magnetic measurements of GdRh_3C [16]. The peaks observed in the $\rho(T)$ data of $x = 0.25, 0.50, 0.75$ and 1.00 compositions are likely due to opening of an AFM superzone pseudo-gap at the Fermi surface that occurs because of a magnetic structure which is incommensurate with the periodicity of the crystal structure [45–50]. To test scenario, we fitted the $\rho_{\text{mag}}(T)$ data for $T_{\text{R}} \leq T \leq 30$ K using $\rho_{\text{mag}}(T) = Ae^{\Delta/k_{\text{B}}T}$, where A is a constant and 2Δ is

the superzone band gap. We obtained reasonable fits for all four compositions. The fitted values of the parameters are listed in Table S1.

DISCUSSION

Our temperature dependent XRD data and their analyses confirm that all the five $\text{GdRh}_3\text{C}_{1-x}\text{B}_x$ compositions are single phase and crystallize in the cubic perovskite structure. While the $\chi(T)$ and $M(H)$ data indicate FM ordering at low temperatures, the substantial evolution of θ_{p} in Fig. 2(c) that increases roughly six times in the boron-end composition compared to the carbon-end composition, suggests that competing magnetic interactions are present in the system, and their resultant strengths vary significantly with changes in composition and lattice parameter. The slightly larger than expected value of μ_{eff} and the anomalous field-dependence of M observed in the $x = 0.25, 0.50$ and 0.75 compositions suggest that the conduction carriers are not only partially polarized but are also coupled in a field-dependent way with the Gd-moments. As these compositions contain both boron and carbon, this remarkable phenomenon is apparently linked with the lattice disorder and the resultant alteration of the local interactions triggered by the substitution.

In this complex system, the $C_{\text{p}}(T)$ and $\rho(T)$ data provide substantial additional information on the nature of the underlying magnetic ground state. The shapes of the low temperature $C_{\text{mag}}(T)$ plots confirm that the magnetic ground states are quite different in the boron- and the carbon-rich compositions. While the former exhibits a λ -shaped peak expected from the equal moment (EM) systems, the latter shows a broad peak with a reduced $\Delta C_{\text{mag}}(T)$ at the magnetic ordering temperature, a behavior which is reported for the amplitude modulated (AM) systems [40–43]. In Ref. 41, Blanco *et al.* estimate that ΔC_{mag} in AM systems is 2/3 of the jump observed in the same in EM systems. Consistent with their estimation, we observe a jump of $\Delta C_{\text{mag}} = 16.6(3)$ J/mol K in the boron-rich compositions and $\Delta C_{\text{mag}} = 11.5(5)$ J/mol K in the carbon-rich compositions. Therefore, the shapes of the $C_{\text{mag}}(T)$ plots as well as the values of the ΔC_{mag} both collectively suggest that the underlying magnetic structure undergoes a transformation from AM-type in $x = 0$ and 0.25 to EM-type in $x = 0.50, 0.75$ and 1.00 compositions (Fig. 9). Furthermore, these results suggest that the $\text{GdRh}_3\text{C}_{1-x}\text{B}_x$ system is energetically positioned near a magnetic tipping point where a small change of the lattice parameter by ≈ 0.005 Å or the electron density by $0.25 e^-/\text{unit cell}$ induced by a change in composition can lead to a substantial alteration in the spin arrangements in their low temperature magnetic structures.

The $S_{\text{mag}}(T)$ of boron-rich compositions ($x =$

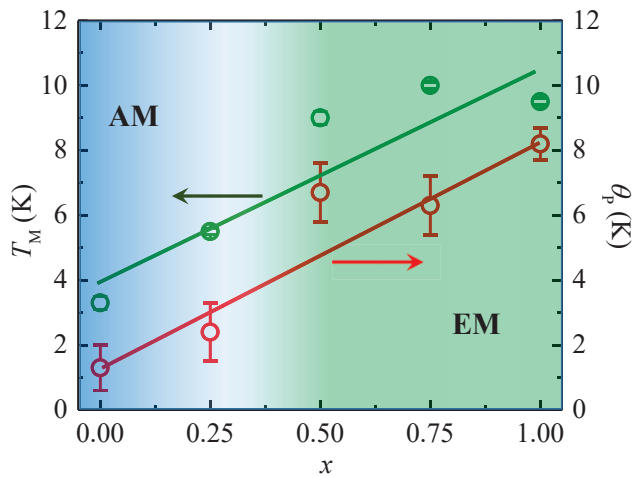


FIG. 9: Magnetic phase diagram of the $\text{GdRh}_3\text{C}_{1-x}\text{B}_x$ system. The left vertical axis shows the variation of magnetic ordering temperature T_M with boron content x and the right vertical axis shows the variation of Weiss temperature θ_p with x . The amplitude modulated (AM) and equal moment (EM) phase regions are indicated. Solid red and green lines are guides to the eye.

0.50, 0.75 and 1.00) saturates to $R\ln 8 = 17.3$ J/mol K, when the low temperature ($T \leq 1.8$ K) C_{mag} is extrapolated as BT^3 assuming the AFM spin wave behavior [Figs. 5(f), (h) and (j)]. However, if we consider a FM spin wave dispersion and extrapolate low- T C_{mag} as $BT^{3/2}$, then $S_{\text{mag}}(T)$ of the same three compositions saturates to the values which are considerably higher than $R\ln 8$ (Fig. S4, Supplementary Materials). This shows that the AFM spin wave description is the correct for these three compositions. One can employ a more accurate expression given in Ref. [38] for the description of low temperature C_{mag} . However, since the simplified BT^3 provides an precise estimate at low temperatures, we have used it in our calculations. As the θ_p decreases with increasing carbon content, it seems more appropriate to use the same AFM spin wave formalism for the extrapolation of low temperature C_{mag} of the carbon-rich ($x = 0$ and 0.25) compositions. However, if we do that, then the $S_{\text{mag}}(T)$ saturates to the values which are significantly smaller than $R\ln 8$ [Figs. 5(b) and (d)], suggesting that the AFM spin wave approximation does not describe the magnetic excitations down to the lowest temperatures in the carbon-rich compositions that show signatures of AM magnetic behavior. Furthermore, even the FM spin wave description does not account for the lost entropy of GdRh_3C (Fig. S4, Supplementary Materials). These observations further infer that not all the Gd-spins are ordering at the respective T_H s of the carbon-rich compositions. This behavior is typical to the AM systems where the amplitude of the ordered magnetic moment varies in a periodic manner right below the magnetic ordering temperature and often evolves to

an EM-type structure at lower temperatures [41]. While neutron diffraction measurements are essential in finding out the exact magnetic structure and its evolution below the magnetic ordering temperature, our $C_{\text{mag}}(T)$ and $S_{\text{mag}}(T)$ data together do provide indications that the underlying magnetic structures in boron-rich compositions ($x = 0.50, 0.75$ and 1.00) are EM-type while the same in carbon-rich compositions ($x = 0$ and 0.25) are AM-type (Fig. 9).

The $\text{GdRh}_3\text{C}_{1-x}\text{B}_x$ materials show a metallic behavior in the electrical transport measurements. The low-temperature $\rho(T)$ data of all the compositions show clear features, either in term of a broad hump observed in the case of GdRh_3C or well-defined peaks observed in the other four compositions. The observation of activated T -dependence $\rho_{\text{mag}}(T) = Ae^{\Delta/k_B T}$ in the boron-rich compositions suggest that the underlying magnetic structure in these systems is an incommensurate AFM type (Fig. 8). The value the prefactor A goes down by a factor of about three in the carbon rich $x = 0.25$ (Table S1). This suggests that the superzone pseudogap starts closing with the increase of the carbon content, and the gap is fully closed with no indication of the activated behavior in GdRh_3C . These results confirm the conclusions achieved from the analysis of the $C_p(T)$ data and show that the magnetic ground states are significantly different in the boron-rich compositions ($x = 0.50, 0.75$ and 1.00) where the magnetic structure is EM-type, and in carbon-rich compositions ($x = 0.00$ and 0.25) which likely have an AM-type magnetic structure.

Therefore, our results show that that while the magnetic measurements indicate a FM ordering in the all the five investigated compositions, the actual ground states are rather complicated and are decisively not a prototypical FM-type. Competing interaction are definitely present in the the $\text{GdRh}_3\text{C}_{1-x}\text{B}_x$ and evolve with substitution. The interplay of the interactions within the localized Gd^{+3} moments as well as between the local moments and the conduction carriers lead to a variety of outcomes such as, field-dependent behavior of conduction carrier polarization, opening of superzone pseudogap and evolution of ground state from AM-modulated type to EM-type. If we consider only the two end compositions, then the magnetic ground states evolves from AM-type in GdRh_3C to incommensurate EM-type in GdRh_3B . It would be interesting to investigate if this evolution is solely triggered by the increase in the lattice parameters and hence the distance between moment-bearing Gd^{+3} ions or the change in the electron density introduced by doping holes in the system by replacing C with B also has a role to play in this mechanism. In either case, this system whose magnetism originates from the S state Gd^{+3} ions that do not have the added complexity of the crystalline electric field effects or the Kondo/heavy fermion behaviors, presents an example of a scenario where the resultant magnetic ground state depends on a delicate

balance of the parameters that are influenced by manipulating the relative content of small and non-magnetic entities.

CONCLUSION

Metallic perovskite materials $\text{GdRh}_3\text{C}_{1-x}\text{B}_x$ show intriguing properties where perturbation caused in the lattice as well as in the electron density by manipulating the relative contents of the metalloids B and C manifests in a very significant transformation in the magnetic ground state—presumably AM-type in GdRh_3C to incommensurate EM-type in GdRh_3B . The observed noteworthy alteration in the ground state which is triggered by small nonmagnetic entities indicates that this system is positioned near a magnetic instability where small alteration in the parameters leads to considerable outcomes. Another remarkable observation is the field-dependent evolution of the conduction carrier polarization, which needs to further explored. Observation of outstanding properties in the oxygen-based as well as in the non-oxide perovskites suggest that we must keep exploring new/unexplored members of this remarkable family.

Acknowledgments

AP acknowledges the support of Wits FRC and URC through the grants 001 254 87581018503 and 001.000.8758101.3113101, respectively. The work at SINP was funded by the Department of Atomic Energy, India. The work at Ames Laboratory was supported by the U.S. Department of Energy, Office of Basic Energy Sciences, Division of Materials Sciences and Engineering. Ames Laboratory is operated for the U.S. Department of Energy by Iowa State University under Contract No. DE-AC02-07CH11358.

* abhishek.pandey@wits.ac.za

- [1] M. A. Pena and J. L. G. Fierro, Chemical Structures and Performance of Perovskite Oxides, *Chem. Rev.* **101**, 1981 (2001).
- [2] P. Szuromi, B. Grocholski, Natural and engineered perovskites, *Science* **358**, 732 (2017).
- [3] T. He, Q. Huang, A. P. Ramirez, Y. Wang, K. A. Regan, N. Rogado, M. A. Hayward, M. K. Haas, J. S. Slusky, K. Inumara, H. W. Zandbergen, N. P. Ong, and R. J. Cava, Superconductivity in the non-oxide perovskite MgCNi_3 , *Nature* **411**, 54 (2001).
- [4] A. Houben, P. Muller, J. von Appen, H. Lueken, R. Niewa, and R. Dronskowski, Synthesis, Crystal Structure, and Magnetic Properties of the Semihard Itinerant Ferromagnet RhFe_3N , *Angew. Chem. Int. Ed.* **44**, 7212 (2005).
- [5] J. von Appen and R. Dronskowski, Predicting New Ferromagnetic Nitrides from Electronic Structure Theory: IrFe_3N and RhFe_3N , *Angew. Chem. Int. Ed.* **44**, 1205 (2005).
- [6] T. M. Gesing, K. H. Wachtmann, and W. Jeitschko, The Perovskite Carbides $A_3\text{MC}$ ($A = \text{Sc, Y, La - Nd, Sm, Gd - Lu}$; $M = \text{Al, Ga, In, Tl, Sn, Pb}$), *Z. Naturforsch.* **52b**, 176 (1997).
- [7] K. Kamishima, M. I. Bartashevich, T. Goto, M. Kikuchi, and T. Kanomata, Magnetic Behavior of Mn_3GaC under High Magnetic Field and High Pressure, *J. Phys. Soc. Jpn.* **67**, 1748 (1998).
- [8] K. Kamishima, T. Goto, H. Nakagawa, N. Miura, M. Ohashi, and N. Mori, Giant magnetoresistance in the intermetallic compound Mn_3GaC , *Phys. Rev. B* **63**, 024426 (2000).
- [9] T. Tohei and H. Wada, Negative magnetocaloric effect at the antiferromagnetic to ferromagnetic transition of Mn_3GaC , *J. Appl. Phys.* **94**, 1800 (2003).
- [10] A. Pandey, C. Mazumdar, R. Ranganathan, S. Tripathi, D. Pandey, and S. Dattagupta, Transverse vibrations driven negative thermal expansion in a metallic compound $\text{GdPd}_3\text{B}_{0.25}\text{C}_{0.75}$, *Appl. Phys. Lett.* **92**, 261913 (2008).
- [11] A. Pandey, C. Mazumdar, R. Ranganathan, M. De Raychaudhury, T. Saha-Dasgupta, S. Tripathi, D. Pandey, and S. Dattagupta, Negative temperature coefficient of resistance in a crystalline compound, *Europhys. Lett.* **84**, 47007 (2008).
- [12] T. Takahashi, R. Iskandar, F. Munnik, D. Music, J. Mayer, and J. M. Schneider, Synthesis, microstructure, and mechanical properties of YPd_3B thin films, *J. Alloys Compd.* **540**, 75 (2012).
- [13] R. Gumeniuk, M. Schmitt, C. Loison, W. Carrillo-Cabrera, U. Burkhardt, G. Auffermann, M. Schmidt, W. Schnelle, C. Geibel, A. Leithe-Jasper, and H. Rosner, Boron induced change of the Eu valence state in EuPd_3B_x ($0 \leq x \leq 0.53$): A theoretical and experimental study, *Phys. Rev. B* **82**, 235113 (2010).
- [14] R. Sahara, T. Shishido, A. Nomura, K. Kudou, S. Okada, V. Kumar, K. Nakajima, and Y. Kawazoe, First-principles study of the structural, electronic, and elastic properties of $\text{RRh}_3\text{B}_xC_{1-x}$ ($R = \text{Sc and Y}$), *Phys. Rev. B* **76**, 024105 (2007).
- [15] D. Music and J. M. Schneider, Influence of valence electron concentration on elastic properties of RRh_3B ($R = \text{Y, Zr, and Nb}$), *Appl. Phys. Lett.* **89**, 121914 (2006).
- [16] D. A. Joshi, N. Kumar, A. Thamizhavel, and S. K. Dhar, Magnetic behavior in RRh_3X ($R = \text{rare earth}$; $X = \text{B, C}$), *Phys. Rev. B* **80**, 224404 (2009).
- [17] M. Djerrouni, S. Kacimi, and A. Zaoui, Electronic and magnetic structure of carbides RRh_3C , *Phys. Stat. Solidi B* **248**, 1925 (2011).
- [18] T. Shishido, K. Kudou, S. Okada, J. Ye, A. Yoshikawa, T. Sasaki, M. Oku, H. Horiuchi, I. Higashi, S. Kohiki, Y. Kawazoe, and K. Nakajima, R -Dependency of the Hardness of Perovskite-Type RRh_3B Compounds ($R = \text{La, Gd, Lu and Sc}$), *Jpn. J. Appl. Phys.* **40**, 6037 (2001).
- [19] A. Pandey, C. Mazumdar, and R. Ranganathan, Observation of giant magnetoresistance and reversal of its sign upon boron filling in cubic TbPd_3 , *Appl. Phys. Lett.* **94**, 172509 (2009).
- [20] A. Pandey, C. Mazumdar, R. Ranganathan, V. R. Reddy, and A. Gupta, Intermediate valency of Eu in a cubic in-

- termetallic compound $\text{Ce}_{0.5}\text{Eu}_{0.5}\text{Pd}_3$, *Appl. Phys. Lett.* **94**, 182503 (2009).
- [21] A. Pandey, C. Mazumdar, and R. Ranganathan, in *Rare Earths: New Research*, edited by Z. Liu (Nova Publishers, New York, 2013).
- [22] O. Elsenhans, P. Fischer, A. Furrer, K. N. Clausen, H. G. Purwins, and F. Hulliger, Incommensurate and commensurate magnetic long-range order in metallic REPd_3 compounds of rare earths (RE = Nd, Tb, Dy, Er, Tm, Yb), *Z. Phys. B* **82**, 61 (1991).
- [23] W. E. Gardner, J. Penfold, T. F. Smith, and I. R. Harris, Magnetic properties of LnPd_3 phases, *J. Phys. F: Met. Phys.* **2**, 133 (1972).
- [24] A. Pandey, C. Mazumdar, R. Ranganathan, and D. C. Johnston, Multiple crossovers between positive and negative magnetoresistance versus field due to fragile spin structure in metallic GdPd_3 , *Sci. Rep.* **7**, 42789 (2017).
- [25] O. Loebich Jr. and E. Raub, Das system gadolinium-rhodium und legierungen des rhodiums mit anderen lathaniden, *J. Less Common Met.* **46**, 1 (1976).
- [26] J. Rodríguez-Carvajal, Recent advances in magnetic structure determination by neutron powder diffraction, *Physica B* **192**, 55 (1993); see also www.ill.eu/sites/fullprof/.
- [27] L. Vegard, Die Konstitution der Mischkristalle und die Raumfüllung der Atome, *Z. Phys.* **5**, 17 (1921).
- [28] T. Shishido, J. Ye, S. Okada, K. Kudou, K. Iizumi, M. Oku, Y. Ishizawa, R. Sahara, V. Kumar, A. Yoshikawa, M. Tanaka, H. Horiuchi, A. Nomura, T. Sugawara, K. Obara, T. Amano, S. Kohiki, Y. Kawazoe, and K. Nakajima, Synthesis, boron-nonstoichiometry and hardness of perovskite-type rare earth rhodium borides RRh_3B_x ($R = \text{La, Gd, Lu and Sc}$), *J. Alloys Compds.* **408-412**, 379 (2006).
- [29] B. N. Harmon and A. J. Freeman, R. G. Jordan, and D. W. Jones, Spin-polarized energy-band structure, conduction-electron polarization, spin densities, and the neutron magnetic form factor of ferromagnetic gadolinium, *Phys. Rev. B* **10**, 1979 (1974).
- [30] L. W. Roelandt, G. J. Cockt, F. A. Mullert, A. C. Molemant, K. A. McEwen, R. G. Jordan, and D. W. Jones, Conduction electron polarization of gadolinium metal, *J. Phys. F: Met. Phys.* **5**, L233 (1975).
- [31] N. Sakai, Y. Tanaka, F. Itoh, H. Sakurai, H. Kawata, and T. Iwazumi, Compton-Profile observation of conduction-electron spin polarization in ferromagnetic Gd, *J. Phys. Soc. Jpn.* **60**, 1201 (1991).
- [32] L. M. Sandratskii and J. Kübler, Local Magnetic Moments of Conduction Electrons in Gadolinium, *Euro. Phys. Lett.* **23**, 661 (1993).
- [33] R. Ahuja, S. Auluck, B. Johansson, and M. S. S. Brooks, Electronic structure, magnetism, and Fermi surfaces of Gd and Tb, *Phys. Rev. B* **50**, 5147 (1994).
- [34] M. Colarieti-Tosti, S. I. Simak, R. Ahuja, L. Nordstrom, O. Eriksson, D. Aberg, S. Edvardsson, and M. S. S. Brooks, Origin of Magnetic Anisotropy of Gd Metal, *Phys. Rev. Lett.* **91**, 157201 (2003).
- [35] A. Pandey, C. Mazumdar, R. Ranganathan, and S. Dattagupta, Magnetism in ordered metallic perovskite compound $\text{GdPd}_3\text{B}_{1-x}\text{C}_x$, *J. Magn. Magn. Mater.* **321**, 2311 (2009).
- [36] A. Pandey, S. L. Samal, and D. C. Johnston, CsMn_4As_3 : A Layered Tetragonal Transition-Metal Pnictide Compound with an Antiferromagnetic Ground State, *Inorg. Chem.* **57**, 3206 (2018).
- [37] N. S. Sangeetha, V. K. Anand, Eduardo Cuervo-Reyes, V. Smetana, A.-V. Mudring, and D. C. Johnston, Enhanced moments of Eu in single crystals of the metallic helical antiferromagnet $\text{EuCo}_{2-y}\text{As}_2$, *Phys. Rev. B* **97**, 144403 (2018).
- [38] D. C. Johnston, Unified molecular field theory for collinear and noncollinear Heisenberg antiferromagnets, *Phys. Rev. B* **91**, 064427 (2015).
- [39] R. J. Goetsch, V. K. Anand, and D. C. Johnston, Antiferromagnetism in EuNiGe_3 , *Phys. Rev. B* **87**, 064406 (2013).
- [40] M. Bouvier, P. Lethuillier, and D. Schmitt, Specific heat in some gadolinium compounds. I. Experimental, *Phys. Rev. B* **43**, 13137 (1991).
- [41] J. A. Blanco, D. Gignoux, and D. Schmitt, Specific heat in some gadolinium compounds. II. Theoretical model, *Phys. Rev. B* **43**, 13145 (1991).
- [42] A. Malachias, E. Granado, R. Lora-Serrano, P. G. Pagliuso, and C. A. Pérez, Spin structure and rst-order transition of GdIn_3 : Near-surface magnetism, buried amplitude-modulated phase, and interface delocalization, *Phys. Rev. B* **77**, 094425 (2008).
- [43] C. Opagiste, R.-M. Galéra, M. Legendre, C. Goujon, S. Pairis, P. Bordet, High-pressure high-temperature synthesis of non-centrosymmetric $\text{R}_3\text{Pt}_4\text{Ge}_{13}$ compounds with $R = \text{Gd, Dy, Ho, Er and Lu}$, *J. Alloys Compd.* **788**, 1211 (2019).
- [44] E. S. R. Gopal, *Specic Heats at Low Temperatures* (Plenum, New York, 1966).
- [45] J. Jensen and A. R. Mackintosh, *Rare Earth Magnetism: Structures and Excitations*, 1st ed. (Clarendon Press, Oxford, 1991).
- [46] R. J. Elliott and F. A. Wedgwood, The temperature dependence of magnetic ordering in the heavy rare earth metals, *Proc. Phys. Soc.* **84**, 63 (1964).
- [47] M. Ellerby, K. A. McEwen, and J. Jensen, Magnetoresistance and magnetization study of thulium. *Phys. Rev. B* **57**, 8416 (1998).
- [48] T. Park, V. A. Sidorov, Hanoh Lee, Z. Fisk, and J. D. Thompson, Pressure-tuned first-order phase transition and accompanying resistivity anomaly in $\text{CeZn}_{1-\delta}\text{Sb}_2$, *Phys. Rev. B* **72**, 060410(R) (2005).
- [49] M. D. Wilding and E. W. Lee, Superzone boundary effects in the electrical resistivity of dysprosium, *Proc. Phys. Soc.* **85**, 955 (1965).
- [50] A. D. Mackintosh, Magnetic ordering and the electronic structure of rare-earth metals, *Phys. Rev. Lett.* **9**, 90 (1962).